Combined deficiency of alpha and epsilon sarcoglycan disrupts the cardiac dystrophin complex

Alessio Lancioni[1], Ida Luisa Rotundo[1], Yvonne Monique Kobayashi[2,3,4,5], Luca D'Orsi[1], Stefania Aurino[1,6], Gerardo Nigro[7], Giulio Piluso[6], Dario Acampora[8], Mafalda Cacciottolo[1], Kevin P. Campbell[2,3,4,5] and Vincenzo Nigro[1,6,]∗

[1]Telethon Institute of Genetics and Medicine, Via Pietro Castellino 111, Napoli 80131, Italy, [2]Howard Hughes Medical Institute, [3]Department of Molecular Physiology and Biophysics, [4]Department of Internal Medicine and [5]Department of Neurology, Roy J. and Lucille A. Carver College of Medicine, University of Iowa, Iowa City, IA 52242, USA, [6]Laboratorio di Genetica Medica, Dipartimento di Patologia Generale and CIRM, Seconda Università degli Studi di Napoli, Napoli, Italy, [7]A.O. Monaldi, Seconda Università di Napoli, Napoli, Italy and [8]Institute of Genetics and Biophysics–CEINGE Biotecnologie Avanzate, Napoli 80145, Italy

Cardiomyopathy is a puzzling complication in addition to skeletal muscle pathology for patients with mutations in β-, γ- or δ-sarcoglycan (SG) genes. Patients with mutations in α-SG rarely have associated cardiomyopathy, or their cardiac pathology is very mild. We hypothesize that a fifth SG, ε-SG, may compensate for α-SG deficiency in the heart. To investigate the function of ε-SG in striated muscle, we generated an *Sgce*-null mouse and a *Sgca*-;*Sgce*-null mouse, which lacks both α- and ε-SGs. While *Sgce*-null mice showed a wild-type phenotype, with no signs of muscular dystrophy or heart disease, the *Sgca*-;*Sgce*-null mouse developed a progressive muscular dystrophy and a more anticipated and severe cardiomyopathy. It shows a complete loss of residual SGs and a strong reduction in both dystrophin and dystroglycan. Our data indicate that ε-SG is important in preventing cardiomyopathy in α-SG deficiency.

INTRODUCTION

Dilated cardiomyopathy is a multi-factor disease associated with both inherited and acquired forms of the disease (1). Specific genetic deficiencies in components of the dystrophin–glycoprotein complex (DGC) are associated with inherited cardiomyopathy (2). In striated muscle, the DGC primarily consists of dystrophin, the syntrophins, α- and β-dystroglycan, α-sarcoglycan (SG) (3), β-SG (4,5), γ-SG (6), δ-SG (7,8) and sarcospan (9). The DGC confers a structural link between laminin-2 in the extracellular matrix and F-actin of the cytoskeleton (10). The DGC is thought to protect muscle cells from contraction-induced injury (11).

The SGs form a transmembrane sub-complex within the DGC (12). Sarcoglycanopathies are associated with mutations in α-, β-, γ- or δ-SG genes, and are responsible for childhood onset of proximal weakness in autosomal recessive limb-girdle muscular dystrophies (LGMD types 2D, 2E, 2F or 2C, respectively) (13). Patients with mutations associated with β-, γ- or δ-SG may or may not develop cardiomyopathy (14,15), whereas patients with mutations in the α-SG either do not display heart problems or else very mild symptoms of cardiac pathology (16). There is a fifth SG called ε-SG (17,18). Highly homologus to α-SG, ε-SG has a broader expression pattern compared with the striated muscle pattern of α-SG, thus the ε-SG protein is part of the vascular smooth muscle SG complex (19). The ε-SG gene is maternally imprinted (20,21), and mutations in the ε-SG gene are associated with the movement disorder myoclonus dystonia, with no skeletal or cardiac muscle involvement (22).

∗To whom correspondence should be addressed. Tel: +39 0815665704; Fax:+39 0815665704; Email: vinnigro@gmail.com

Campbell and colleagues generated mouse models for LGMD2D, 2E and 2F. The mouse model for LGMD2D is deficient for α-SG (*Sgca*-null) (23). The SG−sarcospan complex is disrupted in this mouse, and the dystroglycan complex is disassociated from the DGC (24), leading to muscular dystrophy with either no or very mild cardiomyopathy. Residual β-, γ- and δ-SGs can be detected in *Sgca*-null skeletal muscle and the DGC without α-SG is detected in the *Sgca*-null cardiac muscle (23), which is consistent with the patient data. However, β- and δ-SG-deficient mouse models (*Sgcb* and *Sgcd*-null) not only develop muscular dystrophy but also cardiomyopathy (15,25). There is no detection of residual SGs in these latter mouse models, which is also observed in patients. These data suggest that a SG complex associated with ε-SG exists in striated muscle and that cardiomyopathy develops in β- and δ-SG deficiency because both SG complexes are disrupted.

To understand the role of ε-SG in skeletal and cardiac muscle, we engineered an *Sgce*-null mouse. In addition, to investigate the impact of the concomitant loss of α- and ε-SG, we generated an *Sgca*-;*Sgce*-null mouse that lacks both α- and ε-SGs. *Sgce*-null mice did not display any skeletal or cardiac muscle differences compared with wild-type controls, consistent with myoclonus dystonia patient data. Deficiency in both α- and ε-SGs resulted in muscular dystrophy with progressive necrosis and fibrosis similar to *Sgca*-null mouse skeletal muscle pathology, except that there was no residual staining of the other SGs. Contrary to the lack of a cardiac involvement in the *Sgca*-null mice, the *Sgca*-;*Sgce*-null mice developed dilated cardiomyopathy.

RESULTS

Biochemical analysis of cardiac DGC of wild-type versus *Sgca*-null cardiac muscle

To understand whether ε-SG may have a role in the cardiac dystrophin-associated complex, we performed biochemical analyses of wild-type, *Sgca*-null and MCKeSG/*Sgca*-null mice that overexpress ε-SG in the α-SG-deficient mouse. On sucrose density gradients, the cardiac DGC of *Sgca*-null mice resembled that of wild-type mice, suggesting that the cardiac DGC is still intact due to the presence of ε-SG (Fig. 1A). Indeed, expression of ε-SG in the *Sgca*-null cardiac sucrose gradient was up-regulated on immunoblots (Fig. 1A). Interestingly, overexpression of ε-SG (MCKeSG/*Sgca*-null) striated muscle did not alter the biochemical sucrose density gradient profile of the DGC components (Fig. 1B and C). In contrast, in *Sgcb*-null and *Sgcd*-null mice, the cardiac DGC was completely absent and these animals develop cardiomyopathy (Fig. 1D). The mutation of dystrophin of *mdx* mice did not produce the absence of the SG complex (Fig. 1E) and *mdx* mice do not develop cardiomyopathy until after 1 year of age.

Generation of *Sgce*-null mice and *Sgca*-;*Sgce*-null mice

To generate *Sgce*-null mice, we constructed a targeting vector in which exons 6−9 that encode the transmembrane and Cys-rich domains were replaced by neo and β-gal (Fig. 2A). We used this strategy, since mutations of either the
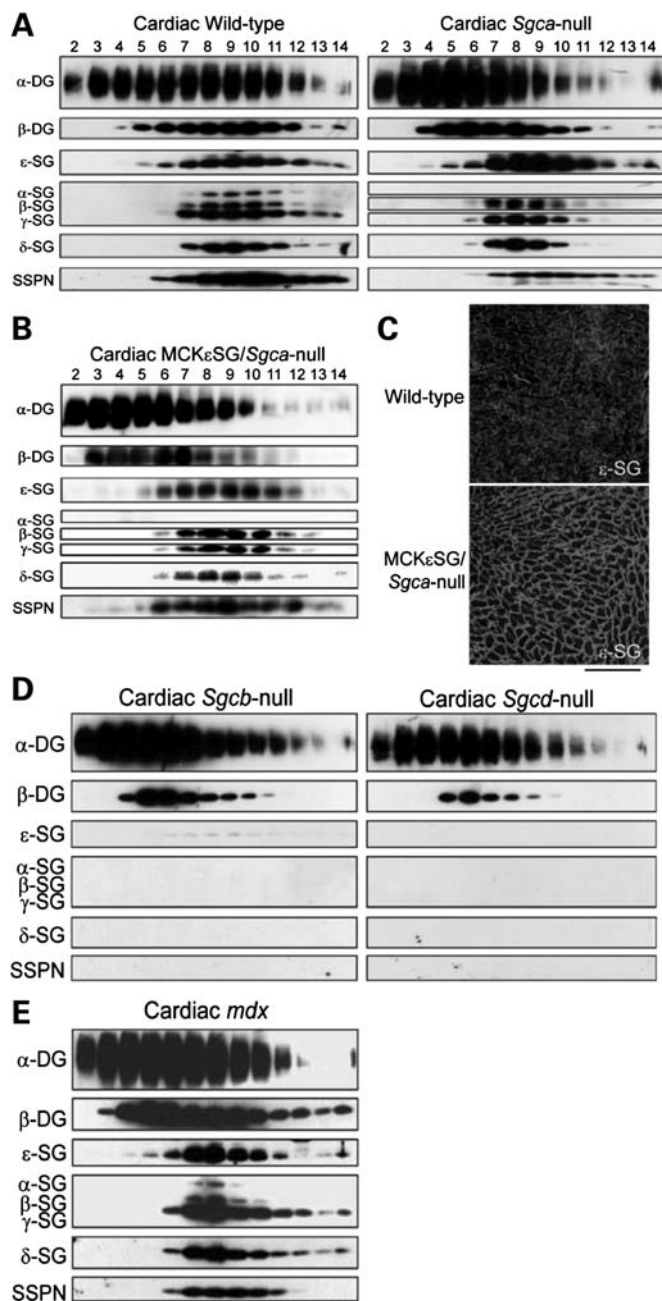

Figure 1. Biochemical analysis. (**A**) Cardiac sucrose density gradient of wild-type mice versus *Sgca*-null mice. On sucrose density gradients, the cardiac DGC of *Sgca*-null mice resembles that of wild-type mice, suggesting that the cardiac DGC is still intact due to the presence of ε-SG. In fact, expression of ε-SG in the *Sgca*-null cardiac sucrose gradient is up-regulated on immunoblots. (**B**) Biochemical figure-cardiac sucrose density gradient of MCKeSG/*Sgca*-null mice. Overexpression of ε-SG in *Sgca*-null striated muscle using the mouse muscle creatine kinase promoter does not alter the biochemical sucrose density gradients profile of the DGC components. (**C**) Immunofluorescent detection of ε-SG on wild-type versus MCKeSG/*Sgca*-null cardiac sections showing that ε-SG is overexpressed. (**D**) Biochemical figure-cardiac sucrose density gradient of *Sgcb*-null and *Sgcd*-null cardiac muscle showing loss of the SG−sarcospan complex in the hearts of these two mouse models, which both develop cardiomyopathy. (**E**) Biochemical figure-cardiac sucrose density gradient of mdx cardiac muscle showing that the cardiac DGC is present (except for dystrophin missing) may explain why mdx mice do not develop cardiomyopathy until after 1 year of age.
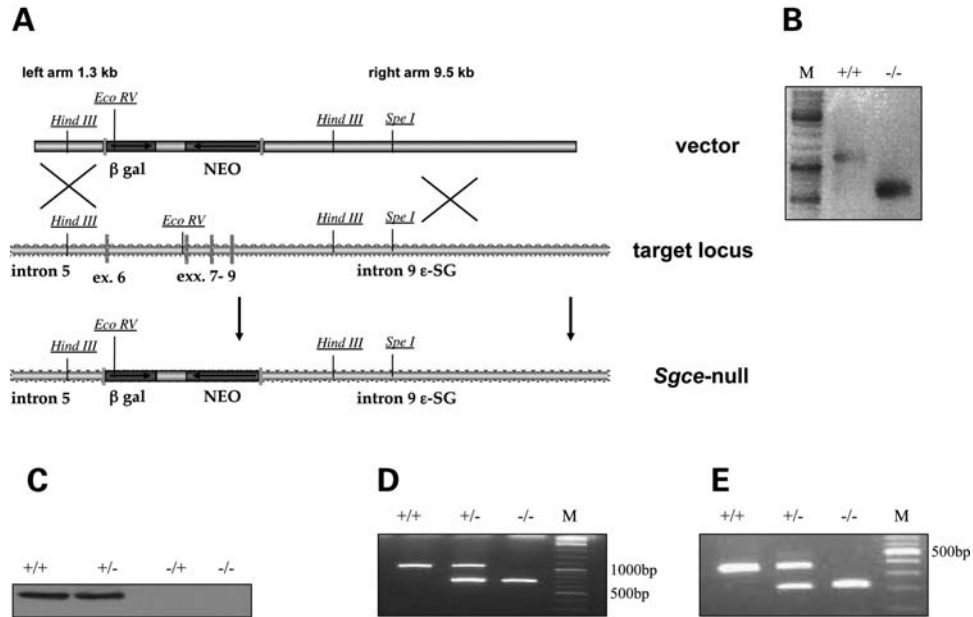
Figure 2. Generation of animal models. (**A**) Homologous recombination was obtained by a vector that replaces exons 6–9 of the mouse ε-SG gene with beta-galactosidase and neo gene. (**B**) 5′RACE that shows the presence of a unique RNA species that joins exons 6–10 in the KO animals only. (**C**) Expression of ε-SG maintains the maternal imprinting following KO. Western blot from the cardiac tissue using anti ε-SG antibody. +/+ indicates WT mice, +/− indicates heterozygous mice that have the mutation on the maternal allele that is not expressed, −/+ indicates heterozygous mice that have the mutation on the paternal allele and the normal allele is not expressed, −/− indicates homozygous mutated mice. (**D**) Allele-specific PCR used to genotype the α-SG mutation produces a 1061 bp and 618 bp for WT and KO, respectively. (**E**) Allele-specific PCR used to genotype the ε-SG mutation produces a 378 bp and 250 bp for WT and KO, respectively.

transmembrane domain or Cys-rich domain of any SG gene generally produce a non-functional allele, while the inactivation of the first exon could activate a cryptic first exon or produce unwanted genomic perturbations. We obtained the homologous recombination in five clones that were checked for possible undesired chromosomal defects. The 133 clones were chosen and chimeras were produced that transmit the mutated ε-SG allele through the germline. We obtained homozygous mice that were crossed with C57BL/6 mice. *Sgce*-null mice were viable and fertile, and they did not present signs of muscular dystrophy.

At least 10 generations of mice were produced, to exclude other co-segregating unwanted alleles and obtain a wild-type background. The homozygous mice do not express ε-SG, but an insignificant amount of mRNA (<1%) was seen by 3′RACE analysis that directly joins exon 5 to exon 10 (Fig. 2B). This transcript is in frame, but no protein was seen. No expression of chimeric ε-SG/neo or ε-SG/β-gal was detected. This confirmed that our *Sgce*-null mice are true null, since they do not express any ε-SG allele. In addition, the correct maternal imprinting was maintained, since the heterozygous *Sgce*$^{-/+}$ mice were also null, when receiving the mutated allele from the male germline (Fig. 2C).

To generate *Sgca*-;*Sgce*-null mice, we crossed our *Sgce*-null mice with the *Sgca*-null homozygous mice (Fig. 2D and E) (23). We first generated double heterozygotes and we crossed them to obtain the homozygotes. Due to the maternal imprinting, the *Sgca*-;*Sgce*-null mice are identical to the *Sgca*-null/*Sgce* heterozygote (+/−) receiving the mutated allele from the male germline.

Sgca-;*Sgce*-null mice show a striking cardiac pathology

To evaluate the effect of the absence of ε-SG and the combined absence of α-SG and ε-SG on the skeletal muscle morphology, we compared hematoxylin and eosin (H&E)—stained sections of the quadriceps and gastrocnemius in wild-type, *Sgce*-null mice, *Sgca*-null mice and *Sgca*-;*Sgce*-null mice between the ages of 2 months and 1 year (Fig. 3A). The *Sgce*-null mice did not show any morphological abnormalities at any of the ages analyzed, while the *Sgca*-null mice and *Sgca*-;*Sgce*-null mice showed extensive pathological alterations already at 2 months of age. The *Sgca*; *Sgce*-null mice showed large necrotic areas, inflammatory infiltration and centralized nuclei comparable with the *Sgca*-null mice. At 1 year of age, lesions worsened in both animal models and severe necrotic areas were observed.

We next examined cardiac tissue. The *Sgce*-null mice were comparable with the wild-type without any fibrotic infiltration at all ages (Fig. 3B). The cardiac muscle of the *Sgca*-null mice at about 6 months of age was characterized by a mild cardiac tissue fibrosis, while the *Sgca*-;*Sgce*-null mice showed an important cardiac pathology characterized by fibrosis and necrotic areas. At 1 year of age, the *Sgca*-;*Sgce*-null mice showed a more severe pathology with a greater number of necrotic areas and fibrotic tissue compared with the *Sgca*-null mice.

The *Sgce*-null mice retain the SG complex

Immunofluorescence analysis was performed for each component of the SG complex on wild-type and *Sgce*-null mice on frozen sections of the quadriceps, gastrocnemius and heart
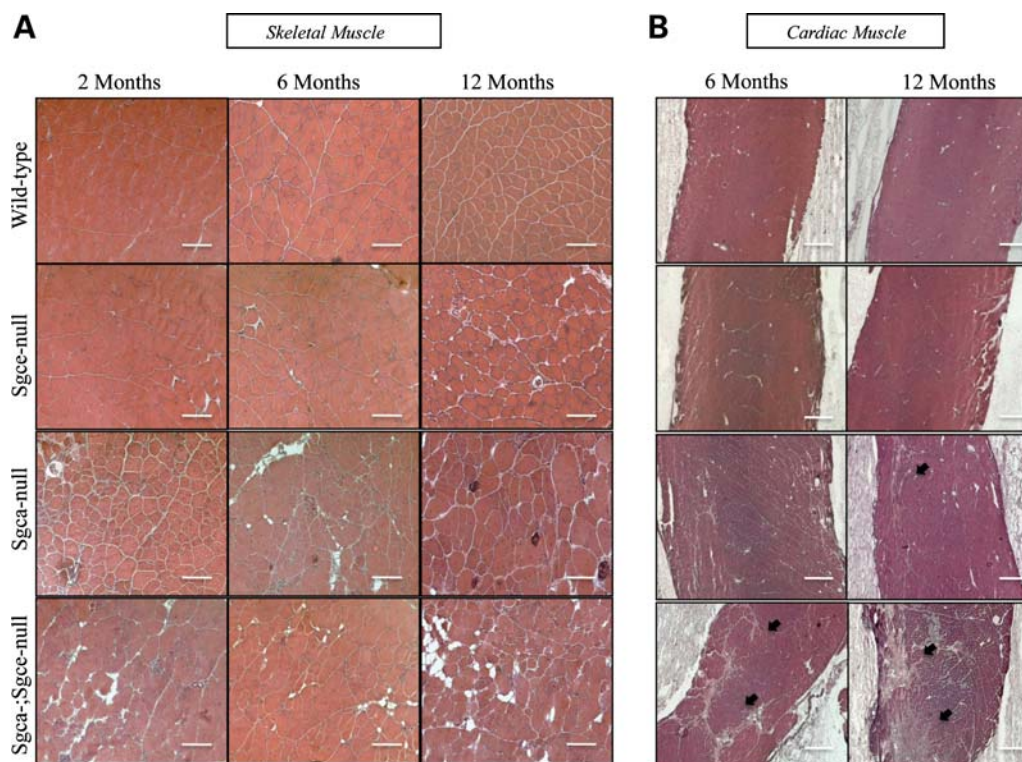
Figure 3. Histological analysis. (**A**) H&E staining of tissue sections from skeletal muscle (quadriceps) and cardiac muscle at the indicated times in the wild-type animal, *Sgce*-null, *Sgca*-null and *Sgca*-;*Sgce*-null. The worsening with time is evident. (**B**) In the cardiac muscle, there is an evident and reproducible worsening of the pathology in the DKO mice when compared with the *Sgca*-null mice. There is no evidence of necrosis in the *Sgce*-null mice.

(Fig. 4A). All the components of the SG complex (δ, β, γ and α) were present and there was no difference in their expression.

We then analyzed the α- and β-dystroglycan and dystrophin and observed the presence of an intact DGC complex.

To measure the amount of the SG and DGC complex, immunoblot analysis was performed on protein membrane preparations for wild-type and *Sgce*-null mice from skeletal and cardiac muscle (Fig. 4B). As expected, ε-SG expression was only detectable in the wild-type mice and was absent in the knock-out animals.

All the others components (δ-, β-, γ- and α-SGs) were present in comparable amounts to the control animals.

The DGC complex was analyzed for β-dystroglycan and dystrophin proteins, and we did not observe any differences between the *Sgce*-null mice and the control animals.

The *Sgca*-;*Sgce*-null mice show an almost complete loss of the DGC

Frozen sections from wild-type, *Sgca*-null mice and *Sgca*-;*Sgce*-null mice from the quadriceps, gastrocnemius and heart were analyzed by immunofluorescence (Fig. 5A and B).

δ-, β- and γ-SGs were greatly reduced in both the *Sgca*-null and *Sgca*-;*Sgce*-null mice, suggesting the secondary loss of the other components of the SG complex in the muscle membrane. α-dystroglycan, β-dystroglycan and dystrophin were also reduced in comparison to wild-type animals, but, interestingly, the *Sgca*-;*Sgce*-null mice dystrophin showed a much stronger reduction compared with the *Sgca*-null mice in which it is already reduced.

The wild-type, *Sgca*-null mice and *Sgca*-;*Sgce*-null mice membrane preparations from the skeletal and cardiac muscle were analyzed by western blot analysis (Fig. 6A). The *Sgca*-null and *Sgca*-;*Sgce*-null mice displayed the absence of α-SG, while we observed the absence of ε-SG only in the *Sgca*-;*Sgce*-null mice. The other components of the SG complex (δ-, β- and γ-SGs) were strongly reduced and we can assume that there was a loss of the SG complex in both animals.

Western blot analysis confirmed what we had observed by immunofluorescence analysis: the reduction is much more evident in the *Sgca*-;*Sgce*-null mice compared with the *Sgca*-null mice and the wild-type. In the same way, the β-dystroglycan and the dystrophin were reduced in the *Sgca*-null animals and strongly reduced in the *Sgca*-;*Sgce*-null mice (Fig. 6B).

To search for ultrastructural alterations, we performed electron microscopy (EM) analyses of wild-type, *Sgce*-null, *Sgca*-null and *Sgca*-;*Sgce*-null mice on skeletal and cardiac muscle at 7 months of age. Mitochondria appeared normal in all models in number and shape. Interestingly, there was a marked disorganization of cardiac muscle fibers and a thickened Z-disk in *Sgca*-;*Sgce*-null mice in comparison with the other mice. This could be related to the effect of concomitant dystrophin–dystroglycan reduction (Fig. 7).

Exercise dramatically worsen the cardiac pathology in the *Sgca*-;*Sgce*-null mice

To evaluate the impact of the major reduction in the SG complex and the dystrophin protein in the *Sgca*-;*Sgce*-
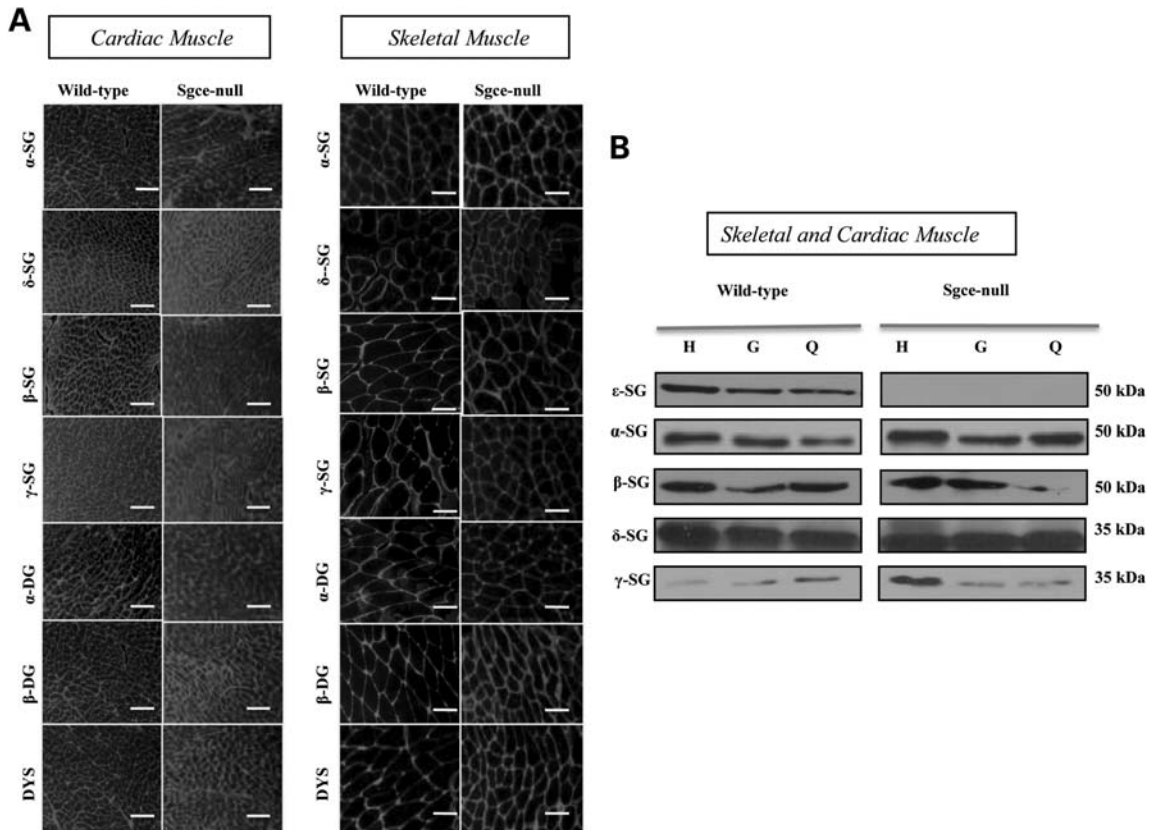
Figure 4. Immunofluorescence and western blot analysis in Sgce-null mice. (**A**) IF using a panel of antibodies (SGs, dystroglycans and dystrophin) in *Sgce-* null mice that confirms the maintenance of all the DGC in the skeletal and cardiac muscle membrane. (**B**) WB analysis, which confirms the absence of *Sgce* and the presence of normal amounts of all the other DGC proteins.

null mice, we exercised wild-type ($n = 6$), *Sgce*-null mice ($n = 6$), *Sgca*-null mice ($n = 6$) and *Sgca*-;*Sgce*-null mice ($n = 6$) starting at 4 months of age using the treadmill.

We generated a control group in rest condition composed of wild-type ($n = 6$), *Sgce*-null mice ($n = 6$), *Sgca*-null mice ($n = 6$) and *Sgca*-;*Sgce*-null mice ($n = 6$) at the same age.

The *Sgce*-null mice showed a performance similar to the wild-type animals, running for 40 min in the first run at 28 cm/s and in the second run at 20 cm/s. In contrast, the *Sgca*-null and *Sgca*-;*Sgce*-null mice, after 2 min at 28 cm/s and 10 min at 20 cm/s were exhausted and they were not able to complete the exercise.

One week after the exercise period, we performed echocardiography analysis (data not shown) and 1 week later we sacrificed three animals from each group for histological analysis.

Interestingly, whole-mount analysis showed a cardiac dilation in the exercised *Sgca*-null mice and *Sgca*-;*Sgce*-null mice (Fig. 8A).

Hystological analysis of the exercised *Sgca*-;*Sgce*-null mice heart revealed extensive alterations including large and numerous foci of necrosis (Fig. 8B), and the Masson Trichrome staining (Fig. 8C) and Evan's blue dye uptake (Fig. 8D) confirmed the presence of fibrotic and necrotic tissue and inflammatory infiltration. No signs of necrosis were present in the exercised *Sgce*-null mice and control animals, and a minor number of necrotic areas characterized the *Sgca*-null mice cardiac tissues. In the groups of animals in rest condition,

the cardiac muscle dimension was normal in the *Sgce*-null and *Sgca*-null mice in comparison to the wild-type animals (data not shown); in the *Sgca*-;*Sgce*-null mice in rest condition, we could observe a cardiac pathology that became more severe after exercise that induced stress and consequent heart damage with a major impact compared with the *Sgca*-null mice. In diaphragm, no substantial difference was observed between *Sgca*-null mice and *Sgca*-;*Sgce*-null mice (Supplementary Material, Fig. S2).

DISCUSSION

In the present paper, we investigated whether or not the heterotetrameric SG complex is composed of functionally equivalent members. Previous observations indicate that *Sgca*-null mice do not develop cardiomyopathy and LGMD2D patients show less severe cardiac involvement than the other forms. First, we biochemically analyzed the sucrose density gradient detection pattern of the cardiac DGC components of wild-type versus *Sgca*-null mice. Despite being α-SG deficient, the sucrose density gradient pattern of the cardiac DGC from *Sgca*-null mice had a similar pattern to that of wild-type mice except that ε-SG appeared up-regulated. The cardiac sucrose density gradient pattern of mice overexpressing ε-SG on an *Sgca*-null background (MCKeSG/*Sgca*-null) (26) was very similar to that of wild-type and *Sgca*-null mice.
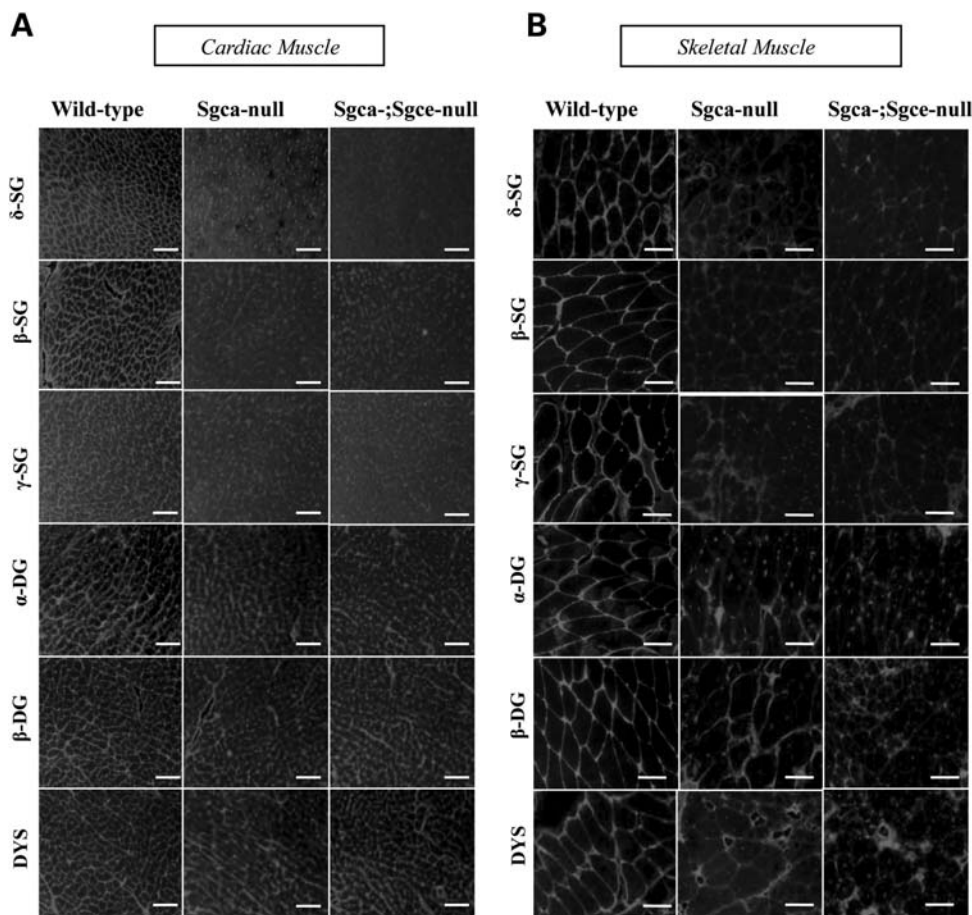
Figure 5. Immunofluorescence analysis in *Sgca* and *Sgca*-;*Sgce*-null mice. (**A**) IF using a panel of antibodies (SGs, dystroglycans and dystrophin) in *Sgca*-null and *Sgca*-;*Sgce*-null mice in both cardiac and (**B**) skeletal muscle. The figures show the absence of the SG complex in both strains and in both tissues, while the reduction in dystroglycan and dystrophin is more severe in the *Sgca*-;*Sgce*-null mice compared with the *Sgca*-null mice. This is more evident in the heart.

To understand the role of ε-SG in the cardiac muscle, we generated two mouse models involving ε-SG: (i) the *Sgce*-null mouse, and (ii) the *Sgca*-;*Sgce*-null mouse by crossing *Sgca*-null (23) and *Sgce*-null mice.

Consistent with patients with mutation in SGCE, *Sgce*-null mice did not show any signs of muscular dystrophy or cardiomyopathy. A different *Sgce*-null mouse was previously reported (21) with prevalent behavioral alterations: differences with our model are possibly linked to the different mutation type.

Disruption of α-SG expression leads to a progressive muscular dystrophy, but without the development of cardiomyopathy in *Sgca*-null mice and rarely in LGMD2D patients. Detection of β-, γ-, and δ-SG residual expression in the *Sgca*-null mouse and patient biopsies suggests that there is another protein that is weakly compensating the α-SG deficiency, which is consistent with α-SG deficiency being the least severe of the sarcoglycanopathies.

However, the complete absence of β-, γ- and δ-SGs in *Sgca*-;*Sgce*-null skeletal and cardiac muscle, but also in smooth muscle vein (Supplementary Material, Fig. S1) supported the idea that ε-SG is the compensating protein. In *Sgca*-;*Sgce*-null skeletal and cardiac muscle, there was a much stronger reduction in dystrophin and dystroglycan expression compared with that of *Sgca*-null mice.

Necrosis and inflammation were more evident in the cardiac tissue from *Sgca*-;*Sgce*-null mice. The latter develop a cardiac disfunction progressing to dilated cardiomyopathy at 6 months of age as measured by echocardiography (Supplementary Material, Table S1). Although some animals undergoing echocardiography were bradycardic for the anesthesia, the signs of cardiomyopathy were observed in *Sgca*-;*Sgce*-null also following a milder physical training (Supplementary Material, Table S1). In contrast, the *Sgce*-null and *Sgca*-null mice maintained normal parameters at this age.

Our data support that ε-SG expression in striated muscle compensates for α-SG deficiency to prevent the development of cardiomyopathy. This compensation could be exerted either by maintaining the SG–sarcospan complex or by maintaining a residual amount of dystrophin and dystroglycan in cardiac muscle and in smooth muscle vein. Interestingly, the requirement of the different SG proteins could be different since the *Sgcg*-null mice also develop a cardiomyopathy, while maintaining residual SG proteins (27). Recently, the importance of maintaining a residual dystrophin in protecting from mechanical stress has been proposed (28). Our data suggest that, at least in mice, ε-SG is an important modifying factor of the cardiomyopathy that develops in sarcoglycanopathies.
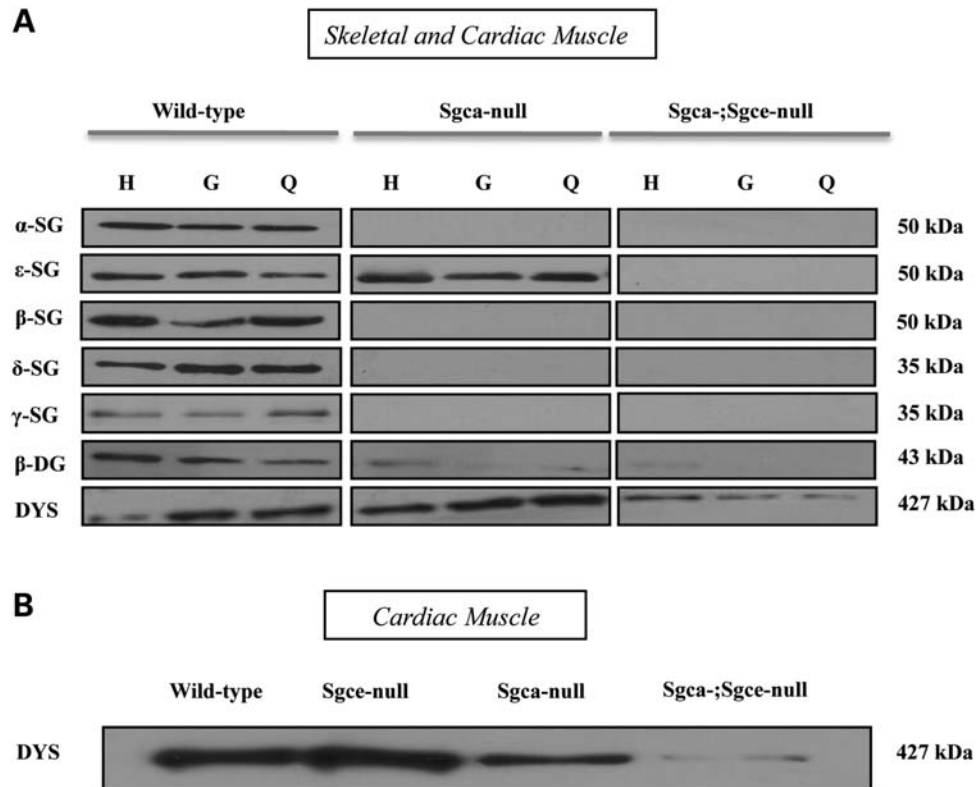
Figure 6. Western blot analysis in *Sgca* and *Sgca-;Sgce*-null mice. (**A**) WB analysis in *Sgca*-null and *Sgca-;Sgce*-null mice in both cardiac and skeletal muscle using antibodies versus α-, β-, γ-, δ-SG, β-dystroglycan and C-terminal dystrophin. The extent of the reduction in the signal of β-dystroglycan and dystrophin in the *Sgca-;Sgce*-null mice compared with the *Sgca*-null mice is much more evident. (**B**) Pool of cardiac tissue belonging to three (5-months old) mice per group to quantify the amount of dystrophin. The strong reduction in dystrophin in the *Sgca-;Sgce*-null mice compared with the *Sgca*-null mice is evident.

MATERIALS AND METHODS

Experimental animals

All mice were housed and handled in accordance with the guidelines of the Institutional Animal Care and Use Committee of I.G.B. Institute of Genetics and Biophysics Naples, Auth. Italy *n.*137/2006-A. Mice were bred for at least 10 generations with C57BL/6 mice to generate and analyze the mutant mice in a pure genetic background. All the other animals used were also in C57Bl6J background.

Vector construction

We amplified a 1.3 kb fragment that comprises intron 5 and a 9.5 kb fragment that comprises intron 9 of the mouse *Sgce* gene from Sv129 DNA. All long-range polymerase chain reactions (PCRs) were performed using proofreading enzymes and a low number of cycles to reduce replication errors. Both fragments were inserted in the same orientation as the neomycin resistance gene and the lacZ reporter gene. Fragments were used to obtain homologous recombination in embryonic stem (ES) cells replacing exon 6–9 with β-gal and neo.

Generation of *Sgce*-null mice

The 16 kb linearized construct was introduced into HM-1 ES cells by electroporation. Positive selection was carried out for 11 days at 350 mg/ml G418. Resistant colonies were picked and DNA was extracted from a fraction (1/5) of the cells for a PCR test of homologous recombination event. Targeting fidelity was determined by vectorette-PCR, sequencing and southern blot analyses. Ten to 15 ES cells were microinjected into C57Bl/6 blastocysts. Injected blastocysts were reimplanted in the uterine horn of pseudopregnant recipient females. Chimeric animals were back-crossed to B6/D2 mice and germline transmission was scored by the presence of agouti coat pigmentation. After germline transmission, the genotypes were determined by PCR on DNA from tail biopsies. The following primers and PCR conditions were used for the epsilon SG: (i) meSG/i5-137F—CAG AGA TGA CTC TAG TTA AGC CCTC; (ii) LacZ3/R—CCA GTC ACG ACG TTG TAA AAC GACG; (iii) meSG/i6+78R— ATG GTA TGT CCA GAC ACA TCA CTGC: initial denaturation at 95°C (7 min) was followed by 35 cycles with denaturation at 95°C (30 s), annealing at 58°C (1 min 30 s) and extension at 68°C for 1 min + 3 s for cycle. All three primers were used in the same PCR reaction. Wild-type and null alleles corresponded to PCR fragments of 378 and 250 bp, respectively.

Sgca-null homozygous mice were obtained from Kevin Campbell. For α-SG, the following primers and PCR conditions were used: (i) INT1 in intron1: CAGGGCTGG GAGCTGGGTTCTG; (b) EX2 in intron 3 (deleted in the null allele): CCCAGGGCCTTGATGCCT; and (iii) NEOTR:
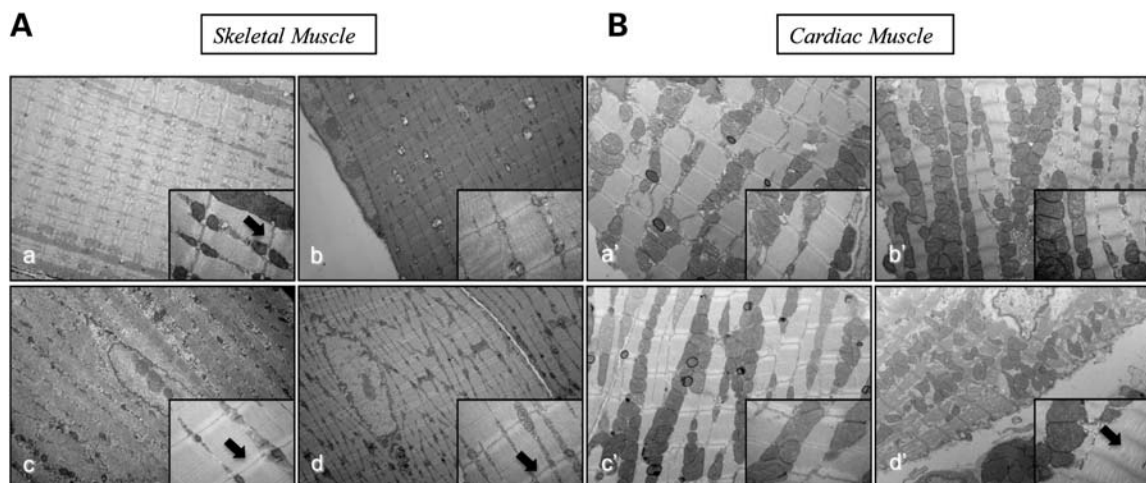
Figure 7. EM analysis. (**A** and **B**) a and a′ (wild-type mice); b and b′ (*Sgce*-null mice); c and c′ (*Sgca*-null mice); and d and d′ (*Sgca*-;*Sgce*-null mice). We notice that there are no evident structural changes in the skeletal muscle, while in the *Sgca*-;*Sgce*- null mice there is an increase in the distance between the fibers in the cardiac muscle.

GCTATCAGGACATAGCGTTGGCTA: first denaturation at 96°C (12 min) was followed by 34 cycles with denaturation at 95°C (30 s), annealing at 64°C (1 min 30 s) and extension at 68°C for 1 min + 3 s for cycle. All three primers were used in the same PCR reaction. Wild-type and null alleles corresponded to PCR fragments of 1061 and 618 bp, respectively.

Generation of *Sgca*-;*Sgce*-null mice

To generate *Sgca*-;*Sgce*-null mice, we crossed our *Sgce*-null mice with the *Sgca*-null mice. We first generated double heterozygotes and crossed them to obtain the homozygotes. Due to the maternal imprinting, the *Sgca*-;*Sgce*-null mice are identical to the *Sgca*-null/ *Sgce* heterozygotes (+/−) with the mutation in the paternal allele. These heterozygous were, however, not used for the experiment here reported: when we indicate '*Sgca*-;*Sgce*-null mice' we always mean the true homozygous animal.

At least 10 generations of mice were produced, to exclude other co-segregating unwanted alleles and a wild-type background.

Race

3′Race was performed from 2 μg of total RNA from the mouse skeletal muscle and heart reverse trascripted (SuperScript III) from the same random oligo T18 5′-gcgaattctagatctcgagg-taccttttttttttttttttttv-3′. First amplification of each cDNA was performed starting from the specific reverse forward primer 5′-agaagaattcccgttgccatatca-3′ located in exon 5 and T18, while the nested PCRs were performed with RACE–LINKER 5′-agcgaattctagatctcgaggtacct-3′ and the specific 5′-ataatgtcagcagaagaattcccgt-3′ located in the 4−5 exon junction.

The PCR reactions were carried out using 20 μl reaction with 0.6 μM of each primer, 3.5 mM dNTP, 1X multibuffer JD (composition available on request) and 0.5 U of AmpliTaq polymerase (Applied Biosystem). Initial denaturation at 99°C (60 s) was followed by 30 cycles with denaturation at 95°C (30 s), annealing at 59°C (30 s) and extension at 68°C for 2 min.

Sucrose density gradients

Glycoprotein enrichment and sucrose gradient fractionation of skeletal and cardiac muscle DGC—cardiac muscle (1.5 g) from wild-type, *Sgca*-, *Sgcb*-, and *Sgcd*-null, MCKeSG/Sgca-null, and *mdx* mice was dissected from mice was solubilized by dounce homogenization in 10−15 ml cold buffer A (50 mM Tris−HCl, pH 7.4, 500 mM NaCl, 1% digitonin) with protease inhibitors (0.6 mg/ml pepstatin A, 0.5 mg/ml aprotinin, 0.5 mg/ml leupeptin, 0.1 mM phenyl methyl sulfonyl fluoride, 0.75 mM benzamidine, 5 mM calpain inhibitor I and 5 mM calpeptin). The homogenate was rotated at 4°C for 1 h, and subsequently spun at 142 400*g* for 37 min at 4°C. The resulting supernatant was pooled and incubated at 4°C with WGA-Agarose (Vector Laboratories). The WGA-Agarose beads were washed extensively in buffer B [50 mM Tris−HCl, pH 7.4, 500 mM NaCl, 0.1% digitonin with protease inhibitors (as above)] and proteins were eluted with 0.3 M N-acetyl glucosamine (Sigma Chemical Co.) in buffer B. The elution was diluted to 50 mM NaCl with 50 mM Tris−HCl, pH 7.4, containing 0.1% digitonin and protease inhibitors (buffer C) and applied to a DEAE-cellulose column, which was subsequently washed in buffer C. The DGC was eluted from the column 500 mM NaCl in buffer C. The 500 mM NaCl fraction was concentrated to 0.4 ml using Centricon 10-filters and applied to a 5−30% sucrose gradient at pH 7.4, as described previously (29).

Antibodies

Monoclonal antibodies from Monosan against alpha SG (Ad1/20A6), β-SG (bSARC/5B1),γ-sarcoglycan (35DAG/21B5), dystrophin C-term (DY8/6C5), β-dystroglycan (43DAG1/885) and α-dystroglycan (via4-1millipore) were used at recommended working dilutions. The polyclonal anti-delta
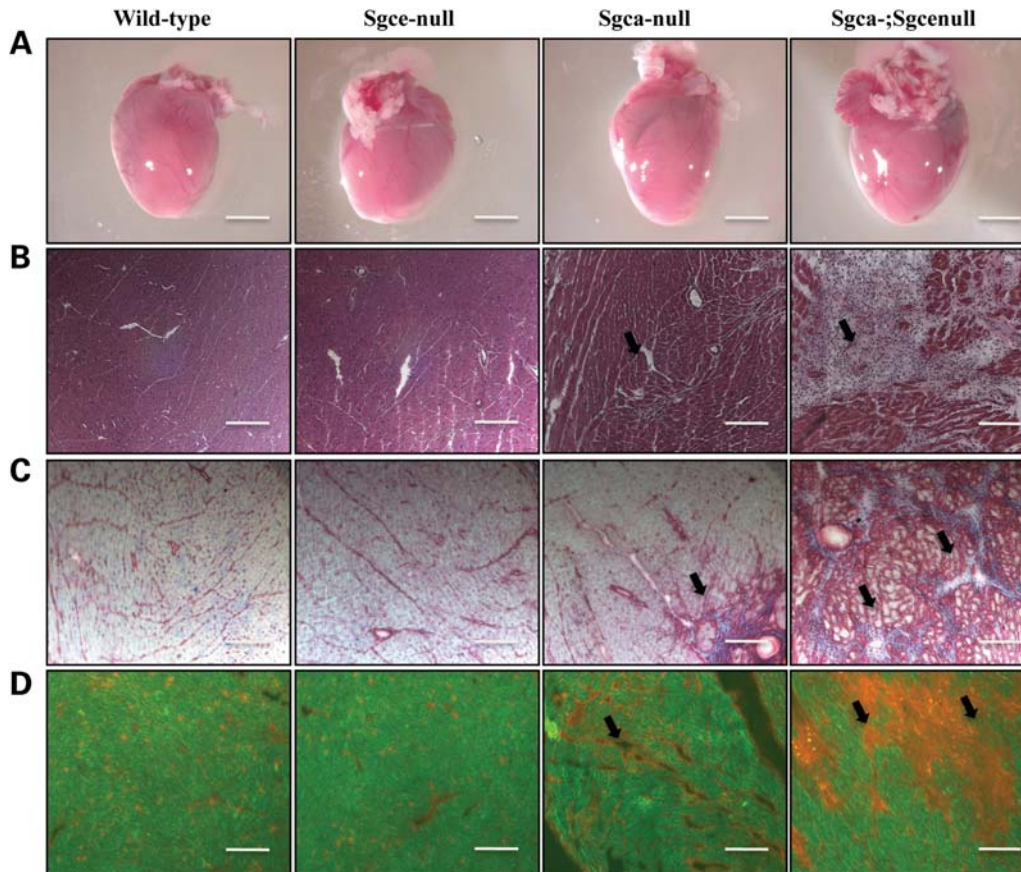
Figure 8. Cardiac analysis. (**A**) Whole-mount, (**B**) H&E staining, (**C**) Masson's trichrome staining, (**D**) Evan's blue dye. The dramatic inflammatory response in the *Sgca-*;*Sgce*-null mice compared with the *Sgca*-null mice is evident following physical exercise on the treadmill.

SG was previously characterized (7) and the polyclonal anti-epsilon SG (R284) was previously described (26). Secondary anti-rabbit Alexa Fluor 568 (Invitrogen) and anti-mouse Alexa Fluor 568 (Invitrogen) were used for immunofluorescence analysis. Horseradish peroxidase-conjugated secondary antibodies from BIORAD were used for western blot analysis.

Hematoxilin and eosin staining (H&E)

The skeletal and cardiac muscle were collected at different ages. The samples were processed by cryosections at 10 μm thickness. The cryosections of the muscular tissues were fixed in 4% paraformaldehyde, then washed in phosphate-buffered saline (PBS-1×) buffer (10 mM Tris–HCl, 200 mM NaCl, 0.05% NP 40, 0.05% TWEEN 20) and stained in haematoxylin for 4 min and in eosin for 6 min. The cryosections were dried in ethanol, fixed in xylene and mounted with the EUKITT mounting kit (O.Kindler GmbH & CO). All sections were acquired under a Zeiss microscope (Carl Zeiss Inc.), using Axio Vision software at a magnification of ×5 and ×10.

Masson's trichrome staining

The cryosections of the muscular tissues were fixed in Bouin's Solution at 56°C for 15 min, cooled and washed in running tap water to remove the yellow color from the sections. They were stained in Working Weigert's Iron Haematoxylin Solution

for 5 min, washed in running tap water for 5 min and stained in Biebrich Scarlet–Acid Fucsin for 5 min, then rinsed in deionised water, placed in Working Phosphotungstic/Phosphomolybdic acid solution for 5 min, stained in Aniline Blue solution for 5 min and in acid acetic 1% for 2 min. All sections were acquired under a Zeiss microscope (Carl Zeiss Inc.), using Axio Vision software at a magnification of ×5 and ×10.

Immunofluorescence analysis

For immunofluorescence analysis, 10 μm transverse cryosections were prepared. The sections were blocked with bovine serum albumin in PBS 1× for 1 h at room temperature and then incubated with a primary antibody overnight at 4°C. After washing with PBS 1×, the sections were incubated with a conjugated secondary antibody (1:300) for 1 h at room temperature and then washed with PBS1X. The sections were mounted with Vectashield with 4′,6-diamidino-2-phenylindole mounting medium (Vector Laboratories, Inc.) and acquired under a Zeiss fluorescence microscope (Carl Zeiss Inc.), using Axio Vision software at a magnification of ×20.

Western blotting

Muscle or other tissues were homogenized in a lyses assay buffer [Urea 8 M, sodium dodecyl sulphate (SDS) 4%, 125 mM Tris–HCl pH 6.8]. The samples were separated on

SDS-10% polyacrylamide gel electrophoresis and transferred to nitrocellulose membrane. After blocking in 10% no fat dry milk in Tween-Tris-buffered saline (TTBS $1\times$) buffer (10 mM Tris–HCl, 150 mM NaCl, 0.05% TWEEN 20) for 1 h, the membranes were incubated with primary antibodies in TTBS $1\times$ at room temperature for 2 h.

Following primary antibody incubation and rinses, the membranes were incubated with the secondary antibody in milk 0.5% and TTBS $1\times$. After 45 min of antibody incubation and five washes with TTBS $1\times$ buffer, the protein band was visualized with a chemiluminescence reagent (Supersignal, WestPico, Pierce) and exposed to X-ray film.

To perform this analysis, Coomassie blue staining was used for the evaluation of the myosin protein expression to understand the variations in the levels of the proteins loaded.

Electron microscopy (EM)

The hearts and muscle (quadriceps muscle) were cut out from WT and KO mice and fixed in 1% glutaraldehyde in 0.2 M 4-(2-hydroxyethyl)-1-piperazineethanesulfonic acid buffer. Then small blocks of the heart and muscle tissue were prepared and post-fixed in OsO_4 and in uranyl acetate. After dehydration in a graded series of ethanol, the tissue samples were cleaned in propylene oxide, embedded in epoxy resin (Epon 812) and polymerized at 60°C for 24 h. From each sample, ultrathin (60 nm thick) sections were cut with a Leica ultracut UCT ultramicrotome. EM images were acquired from thin sections using a JEOL JEM-1011 electron microscope (Tokyo, Japan) equipped with a Morada CCD digital camera. Quantification of the sarcomere and z-line thickness was evaluated using iTEM software (Soft Imaging Systems GmbH, Munster, Germany).

Treadmill

The animals were exercised using the Treadmill (Treadmill Control LE8706—Pamlab Technology), which has an adjustable belt speed (0–80 cm/s) and shock bars with an adjustable amperage (0–2.0 mA). In the first experiment, 4-month-old mice were exercised at 7 cm/s for 5 min to familiarize them with the environment and shock grids, at 15 cm/s for 10 min and at 28 cm/s for the remaining 40 min. One week later, we repeated the treadmill exercising the mice at 7 cm/s for 5 min, at 11 cm/s for 10 min and at 22 cm/s for the remaining 40 min. If an animal became exhausted, the shock bar was turned off and the animal was allowed to rest at the back of treadmill for a short period of time.

SUPPLEMENTARY MATERIAL

Supplementary Material is available at *HMG* online.

ACKNOWLEDGEMENTS

*Conflict of Interest statement*. None declared.

FUNDING

REFERENCES

1. Watkins, H., Ashrafian, H. and Redwood, C. (2011) Inherited cardiomyopathies. *New Engl. J. Med.*, **364**, 1643–1656.
2. Towbin, J.A. (1998) The role of cytoskeletal proteins in cardiomyopathies. *Curr. Opin. Cell Biol.*, **10**, 131–139.
3. Roberds, S.L., Leturcq, F., Allamand, V., Piccolo, F., Jeanpierre, M., Anderson, R.D., Lim, L.E., Lee, J.C., Tome, F.M., Romero, N.B. *et al.* (1994) Missense mutations in the adhalin gene linked to autosomal recessive muscular dystrophy. *Cell*, **78**, 625–633.
4. Lim, L.E., Duclos, F., Broux, O., Bourg, N., Sunada, Y., Allamand, V., Meyer, J., Richard, I., Moomaw, C., Slaughter, C. *et al.* (1995) Beta-sarcoglycan: characterization and role in limb-girdle muscular dystrophy linked to 4q12. *Nat. Genet.*, **11**, 257–265.
5. Bonnemann, C.G., Modi, R., Noguchi, S., Mizuno, Y., Yoshida, M., Gussoni, E., McNally, E.M., Duggan, D.J., Angelini, C. and Hoffman, E.P. (1995) Beta-sarcoglycan (A3b) mutations cause autosomal recessive muscular dystrophy with loss of the sarcoglycan complex. *Nat. Genet.*, **11**, 266–273.
6. Noguchi, S., McNally, E.M., Ben Othmane, K., Hagiwara, Y., Mizuno, Y., Yoshida, M., Yamamoto, H., Bonnemann, C.G., Gussoni, E., Denton, P.H. *et al.* (1995) Mutations in the dystrophin-associated protein gamma-sarcoglycan in chromosome 13 muscular dystrophy. *Science*, **270**, 819–822.
7. Nigro, V., Piluso, G., Belsito, A., Politano, L., Puca, A.A., Papparella, S., Rossi, E., Viglietto, G., Esposito, M.G., Abbondanza, C. *et al.* (1996) Identification of a novel sarcoglycan gene at 5q33 encoding a sarcolemmal 35 kDa glycoprotein. *Hum. Mol. Genet.*, **5**, 1179–1186.
8. Nigro, V., de Sa Moreira, E., Piluso, G., Vainzof, M., Belsito, A., Politano, L., Puca, A.A., Passos-Bueno, M.R. and Zatz, M. (1996)

Autosomal recessive limb-girdle muscular dystrophy, LGMD2F, is caused by a mutation in the delta-sarcoglycan gene. *Nat. Genet.*, **14**, 195–198.

9. Crosbie, R.H., Heighway, J., Venzke, D.P., Lee, J.C. and Campbell, K.P. (1997) Sarcospan, the 25-kDa transmembrane component of the dystrophin-glycoprotein complex. *J. Biol. Chem.*, **272**, 31221–31224.

10. Ervasti, J.M. and Campbell, K.P. (1993) A role for the dystrophin-glycoprotein complex as a transmembrane linker between laminin and actin. *J. Cell Biol.*, **122**, 809–823.

11. Ervasti, J.M. and Campbell, K.P. (1993) Dystrophin and the membrane skeleton. *Curr. Opin. Cell Biol.*, **5**, 82–87.

12. Ozawa, E., Mizuno, Y., Hagiwara, Y., Sasaoka, T. and Yoshida, M. (2005) Molecular and cell biology of the sarcoglycan complex. *Muscle Nerve*, **32**, 563–576.

13. Nigro, V. (2003) Molecular bases of autosomal recessive limb-girdle muscular dystrophies. *Acta Myol.*, **22**, 35–42.

14. Politano, L., Nigro, V., Passamano, L., Petretta, V., Comi, L.I., Papparella, S., Nigro, G., Rambaldi, P.F., Raia, P., Pini, A. *et al.* (2001) Evaluation of cardiac and respiratory involvement in sarcoglycanopathies. *Neuromuscul. Disord.*, **11**, 178–185.

15. Barresi, R., Di Blasi, C., Negri, T., Brugnoni, R., Vitali, A., Felisari, G., Salandi, A., Daniel, S., Cornelio, F., Morandi, L. *et al.* (2000) Disruption of heart sarcoglycan complex and severe cardiomyopathy caused by beta sarcoglycan mutations. *J. Med. Genet.*, **37**, 102–107.

16. Sveen, M.L., Thune, J.J., Kober, L. and Vissing, J. (2008) Cardiac involvement in patients with limb-girdle muscular dystrophy type 2 and Becker muscular dystrophy. *Arch. Neurol.*, **65**, 1196–1201.

17. Ettinger, A.J., Feng, G. and Sanes, J.R. (1997) Epsilon-Sarcoglycan, a broadly expressed homologue of the gene mutated in limb-girdle muscular dystrophy 2D. *J. Biol. Chem.*, **272**, 32534–32538.

18. McNally, E.M., Ly, C.T. and Kunkel, L.M. (1998) Human epsilon-sarcoglycan is highly related to alpha-sarcoglycan (adhalin), the limb girdle muscular dystrophy 2D gene. *FEBS Lett.*, **422**, 27–32.

19. Straub, V., Ettinger, A.J., Durbeej, M., Venzke, D.P., Cutshall, S., Sanes, J.R. and Campbell, K.P. (1999) Epsilon-sarcoglycan replaces alpha-sarcoglycan in smooth muscle to form a unique dystrophin-glycoprotein complex. *J. Biol. Chem.*, **274**, 27989–27996.

20. Grabowski, M., Zimprich, A., Lorenz-Depiereux, B., Kalscheuer, V., Asmus, F., Gasser, T., Meitinger, T. and Strom, T.M. (2003) The epsilon-sarcoglycan gene (SGCE), mutated in myoclonus-dystonia syndrome, is maternally imprinted. *Eur. J. Hum. Genet.*, **11**, 138–144.

21. Yokoi, F., Dang, M.T., Li, J. and Li, Y. (2006) Myoclonus, motor deficits, alterations in emotional responses and monoamine metabolism in epsilon-sarcoglycan deficient mice. *J. Biochem.*, **140**, 141–146.

22. Zimprich, A., Grabowski, M., Asmus, F., Naumann, M., Berg, D., Bertram, M., Scheidtmann, K., Kern, P., Winkelmann, J., Muller-Myhsok, B. *et al.* (2001) Mutations in the gene encoding epsilon-sarcoglycan cause myoclonus-dystonia syndrome. *Nat. Genet.*, **29**, 66–69.

23. Duclos, F., Straub, V., Moore, S.A., Venzke, D.P., Hrstka, R.F., Crosbie, R.H., Durbeej, M., Lebakken, C.S., Ettinger, A.J., van der Meulen, J. *et al.* (1998) Progressive muscular dystrophy in alpha-sarcoglycan-deficient mice. *J. Cell Biol.*, **142**, 1461–1471.

24. Straub, V., Rafael, J.A., Chamberlain, J.S. and Campbell, K.P. (1997) Animal models for muscular dystrophy show different patterns of sarcolemmal disruption. *J. Cell Biol.*, **139**, 375–385.

25. Coral-Vazquez, R., Cohn, R.D., Moore, S.A., Hill, J.A., Weiss, R.M., Davisson, R.L., Straub, V., Barresi, R., Bansal, D., Hrstka, R.F. *et al.* (1999) Disruption of the sarcoglycan-sarcospan complex in vascular smooth muscle: a novel mechanism for cardiomyopathy and muscular dystrophy. *Cell*, **98**, 465–474.

26. Kobayashi, Y.M., Rader, E.P., Crawford, R.W., Iyengar, N.K., Thedens, D.R., Faulkner, J.A., Parikh, S.V., Weiss, R.M., Chamberlain, J.S., Moore, S.A. *et al.* (2008) Sarcolemma-localized nNOS is required to maintain activity after mild exercise. *Nature*, **456**, 511–515.

27. Hack, A.A., Lam, M.Y., Cordier, L., Shoturma, D.I., Ly, C.T., Hadhazy, M.A., Hadhazy, M.R., Sweeney, H.L. and McNally, E.M. (2000) Differential requirement for individual sarcoglycans and dystrophin in the assembly and function of the dystrophin-glycoprotein complex. *J. Cell Sci.*, **113**, 2535–2544.

28. Townsend, D., Yasuda, S., McNally, E. and Metzger, J.M. (2011) Distinct pathophysiological mechanisms of cardiomyopathy in hearts lacking dystrophin or the sarcoglycan complex. *FASEB J*, **25**, 3106–3114.

29. Ervasti, J.M., Kahl, S.D. and Campbell, K.P. (1991) Purification of dystrophin from skeletal muscle. *J. Biol. Chem.*, **266**, 9161–9165.
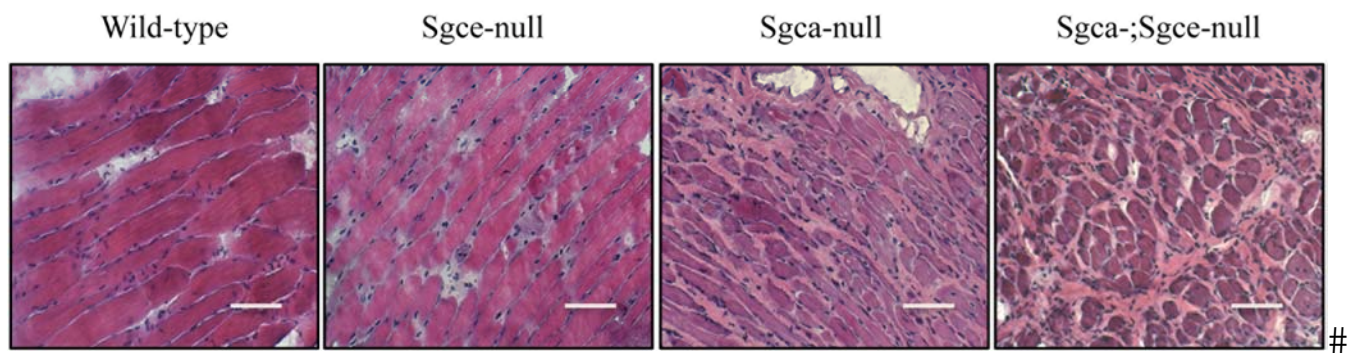
#

Supplementary Figure 1
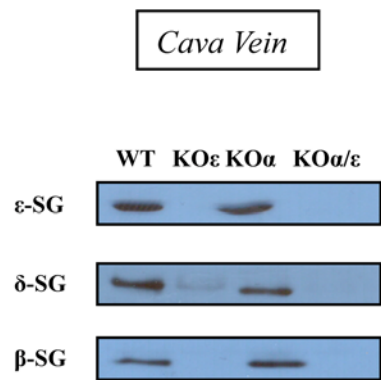
Supplementary figure 1. The DGC complex in smooth muscle of cava vein is detect only in wild-type (WT) and *Sgca*-null mice (KOα), where the ε-SG complex is not lost, while it is strongly reduced ora absent in *Sgce*-null (KOε) and *Sgca-;Sgce*-null mice (KOα/ε).

\#

Supplementary Figure 2

Diaphragm

\#

\#

Supplementary figure 2. The diaphragm histopathology in Wild-type, *Sgce*-null, *Sgca*-null, and *Sgca-;Sgce*-null mice.

Supplementary Table 1

Parameters	Wild-type	*Sgce*-null	*Sgca*-null	*Sgca*-;*Sgce*-null
HR (beats/min)	269 ± 37	295 ± 52	215 ± 46	221 ± 40
IVST (mm)	0.63 ± 0.05	0.73 ± 0.07	0.65 ± 0.11	0.65 ± 0.04
LVEDd (mm)	3.81 ± 0.4	3.64 ± 0.12	3.78 ± 0.27	4.13 ± 0.64 (p= 0.25)
LVESd (mm)	2.59 ± 0.41	2.36 ± 0.23	2.58 ± 0.19	3.15 ± 0.5 (p = 0.04)
FS (%)	32.4 ± 4.2	35.1 ± 8.1	31.4 ± 10.9	23.8 ± 2.9 (p = 0.0006)
EF (%)	61.0 ± 5.9	64.8 ± 9	59.4 ± 11	47.9 ± 5.1 (p =0.001)
number	5	5	5	5

Supplementary Table 1. Echocardiographic study

Echocardiographic parameters in different groups of mice examined at six months of age. These mice were previously exercised at 4

months of age following the standard protocol described under Methods, but without forcing animals to complete any exercise and

allowing sufficient time (up to 1 week) to recovery. Note: these groups are not the same presented in Results.

 HR= heart rate; IVST = Inter Ventricular Septal Thickness; LVEDd = Left Ventricular End Diastolic Diameter; LVESd = Left

Ventricular End Systolic Diameter; FS = Fractional Shortening; EF = Ejection fraction. Data are presented as mean ± SEM.

Methods

Mice were anaesthetized with isoflurane gas that was administered with the use of a vaporizer over a 1-min period in an isolation chamber with 5.0% Isf in 100% O2. The anesthesia was maintained during spontaneous breathing of 1.25% Isf in 100% O2 at a flow rate of 1 l/min. Left parasternal and left apical echocardiographic images of anaesthetized animals lying in the dorsal recumbent position were obtained using the GE Vivid 7 (General Electric, VingMed, Horten, Norway) and an high-frequency probe (30-Mhz). Care was taken to avoid applying excessive pressure, which can induce bradycardia and cardiac arrest. 1-cm region of interest was expanded, allowing high frame rates, and the gain and compression were set for optimal imaging. The chest hair was removed with a topical depilatory agent. All echocardiographic measurements were performed, according to the American Society of Echocardiography recommendations, by the same investigator (G.N.) blinded to mice genotype. For intra- and inter-observer variability of analysis, all images were digitally stored and reviewed off-line by and independent observer who had experience in echocardiographic analysis of rodent heart. The three-lead electrocardiogram (ECG) was recorded from the front limbs and the right hind limb. Two-dimensional guided M-mode imaging was used to measure the LV end-systolic (LVESd) and end-diastolic (LVEDd) diameters, interventricular septal thickness (IVST) during diastole and posterior wall thickness (PWT) during diastole, all in the short-axis view at the level of the papillary muscles. The angle of interrogation of the M-mode beam was carefully aligned to be perpendicular to the LV walls at the antero-posterior axis; LVEDd, IVST and PWT were measured by the leading edge method, and the LVESd was measured at the posterior wall's time of maximum anterior motion. Three representative cardiac cycles were

analyzed and the mean values for each measurement were recorded. LV systolic function was assessed by ejection fraction (EF; %), calculated from these measurements by an automated computer program which displays the output as EF and by fractional shortening (FS; %) which was calculated from the M-mode echocardiogram using the equation defined as (LVEDd - LVESd) / LVEDd x 100. Significance was assessed using unpaired t-test.

#